Available online at www.sciencedirect.com
ScienceDirect
Journal of the European Ceramic Society 29 (2009) 1331–1336
www.elsevier.com/locate/jeurceramsoc

Laser scanning parameters on fabrication of ceramic parts by liquid phase sintering

Hsiao-Chuan Yen [a,1], Ming-Lu Chiu [b,1], Hwa-Hsing Tang [a,*]

[a] *Department of Mechanical Engineering, National Taipei University of Technology, Taipei 10608, Taiwan*
[b] *Graduate Institute of Mechanical and Electrical Engineering, National Taipei, University of Technology, Taipei 10608, Taiwan*

Received 29 April 2008; received in revised form 25 August 2008; accepted 27 August 2008
Available online 25 October 2008

Abstract

Layer manufacturing for fabricating ceramic parts has been carried out by a wet process known as Ceramic Laser Sintering; the process employed ceramic slurry comprised of silica powder, clay, silica gel, and water. The aim of the present research is to establish a systematic method for measuring the width and depth of the scan line on the ultra-thin layer sintered with the laser scanning. Besides laser power and scan speed, laser beam diameter was also included as one of the significant scanning parameters. Furthermore, to optimize the scanning process, a 'critical point' was defined. The working temperature at the critical point is near the melting point of the silica powder. By varying the laser power, the scan speed, and the beam diameter, the optimized scanning parameter combinations can be obtained to produce a series of critical line depths at the critical points. Based on the critical line depth, a proper layer thickness for fabricating sintering part can be determined. Parts possessed inter-connective porous structure, better surface quality, and higher strength can be obtained by employing the optimized scanning parameter combinations.

Keywords: Sintering; Surfaces; Strength; SiO_2; Rapid prototyping

1. Introduction

Due to rapid increase of the need of functional parts, the focus of rapid prototyping technologies has been switched from polymer to metal and ceramic. A variety of techniques, such as stereolithography (SL),[1–4] fused deposition modeling (FDM),[5,6] laminated object manufacturing (LOM),[7–9] selective laser sintering (SLS),[10–12] three-dimensional printing (3DP),[13–15] is capable of producing complex-shaped ceramic components. Most processes employ a polymer to glue the ceramic powders together to fabricate a part. However, Wirtz[12] fabricated a ceramic part by employing a laser to fuse zirconium silicate ($ZrSiO_4$) powder without using any polymeric binder. In his powder-based process, once the grain size of the powder is too small, movability of powder will deteriorate during layer casting; therefore, the layer thickness is hardly thinner than 50 μm and the surface roughness of the fabricated part was 42–54 μm (R_z).

Tang[16–19] invented two processes, Ceramic Laser Fusion (CLF) and Ceramic Laser Sintering (CLS), in 2001 and 2007, respectively. Both processes have identical manufacturing steps and are capable of building ultra-thin layers.[20,21] Instead of using loose powder in SLS, CLF and CLS employ slurry which is comprised of ceramic powder, inorganic binders, and water. Fig. 1 illustrates the entire fabrication process of the ceramic parts. A green layer is formed after layer casting and drying. By tracing the geometry of the cross-section of an object on the surface of the green layer with a laser beam, the temperature of the ceramic powder rises instantaneously to the melting point; the scanned powder is fused and then solidified right after the laser scanning. The steps of laser scanning and layer casting are repeated until the ceramic part is completely fabricated by binding the successive green layers. More details about the manufacturing system and the process can be found elsewhere.[18–21] CLF and CLS provide the advantages of building thin layer with slurry and withstanding the shear stress during the layer casting; moreover, the dried green part can inherently form a strong solid support

* Corresponding author. Tel.: +886 2 27712171x2030; fax: +886 2 27317191.
E-mail address: hhtang@ntut.edu.tw (H.-H. Tang).
[1] Address: No. 1, Chung Hsiao East Road, Sec. 3, Taipei 10608, Taiwan.

0955-2219/$ – see front matter © 2008 Published by Elsevier Ltd.
doi:10.1016/j.jeurceramsoc.2008.08.035

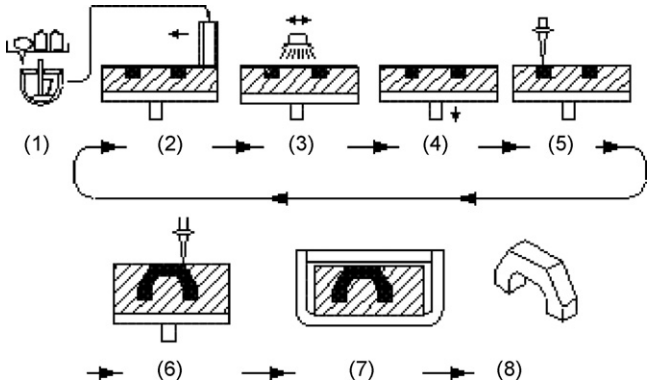

Fig. 1. The schematic representation of entire process of CLF and CLS in fabrication of the ceramic part. (1) Slurry preparation and delivery; (2) layer casting; (3) layer drying; (4) working platform descending; (5) selective laser scanning; (6) process repeating from step 1 to step 5 until part being completed; (7) green part removal in solvent; (8) 3D part completing.

for overhanging geometries of an object. The strong binding force of the solid support can also prevent upward deformation of the built layer; therefore, a layer thinner than 10 μm can be constructed. CLF is somewhat similar to SLS in the principle; nevertheless, scanning with high energy density will lead to depression causing rough surface. To avoid this drawback, CLS applies the principle of liquid phase sintering, and uses a lower energy density. Its working temperature is between the low melting point of the inorganic binder and the high melting point of the structural ceramic powder. Binding is obtained by using the melted inorganic binder to grasp the un-melted ceramic powder. The surface roughness of the sintered part can be around 20 μm (R_z),[21] which is much better than Wirtz's work and parts made by CLF.

In the CLS process, the depth of the scan line (property transformation depth, D_{pt}) should vary with layer thickness to avoid the presence of fusion. According to the previous experimental results, the overlap of the line depth to bind two adjacent layers must be around 50%; therefore, with regard to a layer thickness of 10 μm, which is the minimum layer thickness feasible to fabricate a part by CLF or CLS, the corresponding line depth should be about 20 μm. In other words, if the layer is very thin, the line depth should also be very small. Such thin layer embedded in the solid green part is considerably weak and hard to be taken out from the green part without damage. In order to study the laser scanning process of CLS, it is indispensable to design and build a proper specimen for correctly measuring the width (property transformation width, W_L) and the depth of the scan line.

Although fabricating a ceramic sintering part with CLS brings several advantages, methods for measuring the dimensions of the scanned thin layer have not yet to be developed. Consequently, the present article concentrates on the process of laser scanning to establish a systematic method for fabricating thin property transformation layers and for measuring the geometry of the scan line (W_L and D_{pt}). We have also investigated the relationship between the scanning parameters (laser power (P_L), scan speed (V_s) and beam diameter (d_0)) of the liquid phase sintering and the geometry of the scan line. Afterwards, an optimization of the laser scanning parameters used to obtain a stronger part was conducted. The present study is especially helpful in constructing a laser scanning knowledge base for the fabrication of ceramic sintering parts.

2. Experiment

2.1. Slurry preparation

In order to fulfill the requirements of liquid phase sintering, the slurry used in CLS consisted of high melting point silica powder (melting point ~ 1720 °C) as a structural material, low melting point clay (Wyoming Bentonite clay, melting point ~ 1200 °C) and silica sol (Nissan Chemical SNOWTEX® ST-40, melting point ~ 1700 °C) as inorganic binders, and water as a solvent. After laser scanning, clay particles are melted and flows into pores formed by the un-melted silica powder; the melted clay bridges particles together to build an interconnective porous structure.

A specified proportion of silica sol to clay should be maintained. Although the silica sol enhances the strength of the layers, the dried silica sol is insolvable, and therefore only a minimal amount can be contained in the green part. On the other hand, the dried clay retained in the green part is easily dissolved in water; this characteristic is useful in weakening the binding of the green part which consists of clay and silica sol. Consequently, the proper proportion of silica sol to clay must be maintained. In the present study, the slurry composition was 52.63 wt% silica, 3.68 wt% clay, 1.58 wt% silica sol, and 42.11 wt% water.

2.2. Laser scanning

Preliminary experiments involving laser scanning process in CLS have been reported.[19,20] Besides laser power and scan speed, beam diameter, which varies with the distance between the scanning surface and lens focus (de-focus distance (D_{df})), is also characterized as a significant parameter in the present article.

If the part is fabricated at a temperature between the melting point of the silica powder and the melting point of the clay, the molten clay particles will bind the solid silica powder. The part fabricated with this principle is defined as a liquid phase sintering part. In this paper, the word *sintering* is used instead of *liquid phase sintering* for simplification.

Moreover, the present study also defines a 'critical point' on the working curve built by varying the scanning parameter combination. Fig. 2 represents the working curve constructed by varying the scan speed in conjunction with a constant-beam-diameter and a constant-laser-power. The point, which represents a small part of silica powder at the center of the laser beam begins to melt when a certain scan speed is reached, is called the 'critical point'. The working temperature at this point is quite close to the melting point of the silica powder. When the scan speed slows down further, more silica powder is melted and the working curve entering a range called the "partial fusion phase", because part of the silica powder is fused. The parts fabricated at the working points located on the right side of the critical point are in the "sintering phase"; the silica powder is

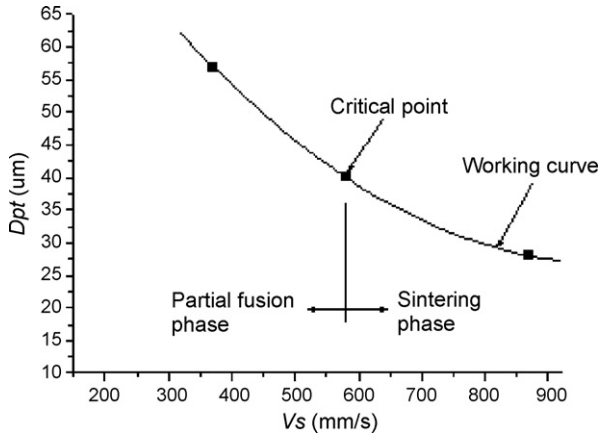

Fig. 2. The working curve built by varying the scan speed in conjunction with a constant-beam-diameter and a constant-laser-power.

not melted but bound by the melted clay. The line depth varies with the scan speed; the slower the scan speed is, the greater the line depth and the higher the scanning surface temperature will be.

After scanning, the green part that transfers to be a sintering or partial fusion part can be observed by a SEM. From the surface and the cross-section of the scanned green part, the binding mechanism can be recognized by observing the melting condition of the silica powder and the clay.

The scanning experiments were designed to measure the line width and the line depth on the specimens fabricated with the following different parameter combinations.

The laser power was increased from 7 W to 18 W at intervals of 1 W; three beam diameters (0.12 mm, 0.17 mm, and 0.19 mm) and three scan speeds (370 mm/s, 580 mm/s, and 870 mm/s) were selected. Each parameter combination was employed to fabricate six specimens. The line width and the line depth represent the average of the measured line width and line depth.

2.3. Line width and line depth measurement

Fig. 3 shows the schematic view of the specimen for measuring the line width. A green layer with a thickness of 20 μm was fabricated on a pre-fabricated solid base with a thickness of 0.5 mm. At a specified de-focus distance, four separated scan lines with assigned laser power and scan speed were built. After removing the green part surrounding the scan lines, the specimens were dried at room temperature, and then placed on an *X–Y* platform equipped with two digital micrometer heads (Mitutoyo 350, resolution 0.001 mm) to measure the width of each scan line by an optical microscope (Nikon SMZ1500). By varying the de-focus distance to change the beam diameter, other specimens can be fabricated accordingly.

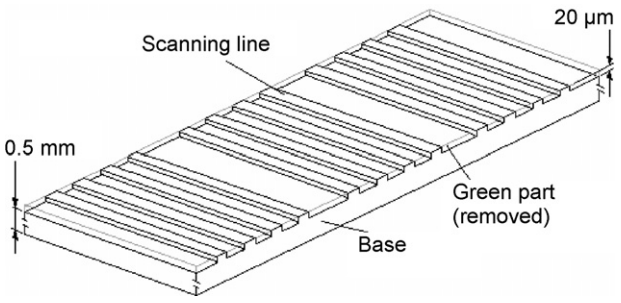

Fig. 3. The schematic view of the specimen for measuring the line width.

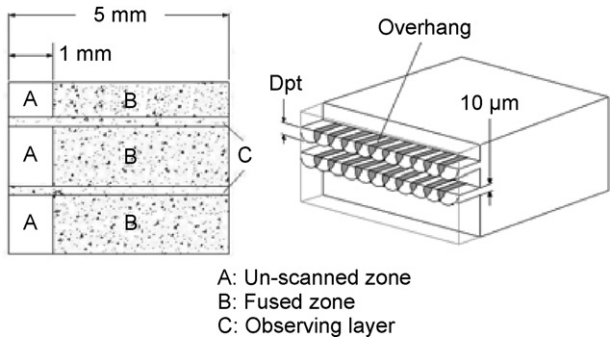

Fig. 4. The schematic view of the specimen for measuring the line depth.

Fig. 4 is the schematic view of the specimen for measuring the line depth. In order to obtain the line depths at different scanning parameter combinations, a specimen having two 1 mm overhangs was fabricated. The specimen was made layer by layer; the layer thickness was 50 μm. To ensure that each layer could be bound to the previous layer, layers in zone B were fused; however, zone A was still retained the green state. Two separated observing layers (zone C) were fabricated at a specified scanning parameter combination as mentioned in Section 2.2. The thickness of each observing layer was 10 μm. Most line depths in the present study was between 20 μm and 50 μm; therefore, based on the 50% overlap, the thickness of the observing layer should not be greater than 10 μm to ensure a good binding to the previous layer at each scanning parameter combination. After removing the green part (zone A), the specimen was dried and placed on an *X–Y* platform to measure the depth of overhang (the depth of scan line) by using an optical microscope. By varying the parameter combination, other specimens can be fabricated accordingly.

3. Results and discussion

3.1. Microscopic topography of specimens

We observed the surfaces of specimens fabricated for the measurement of the line width (Fig. 3) with a scanning electron microscope (SEM). The surfaces had different topographies as shown in Fig. 5 and implied that they were produced by different binding mechanisms. The micrographs shown in Fig. 5(a–c) were taken from the specimens fabricated with constant-laser-power, constant-beam-diameter, and a decrease in scan speed. The micrograph in Fig. 5(a) was taken from a specimen fabricated with the highest scan speed. The silica powder did not melt and the specimen did not collapse in water; therefore, it is reasonable to infer that the surface working temperature is above the melting point of the clay but much lower than the melting point of the silica powder. The specimen of Fig. 5(a) had the

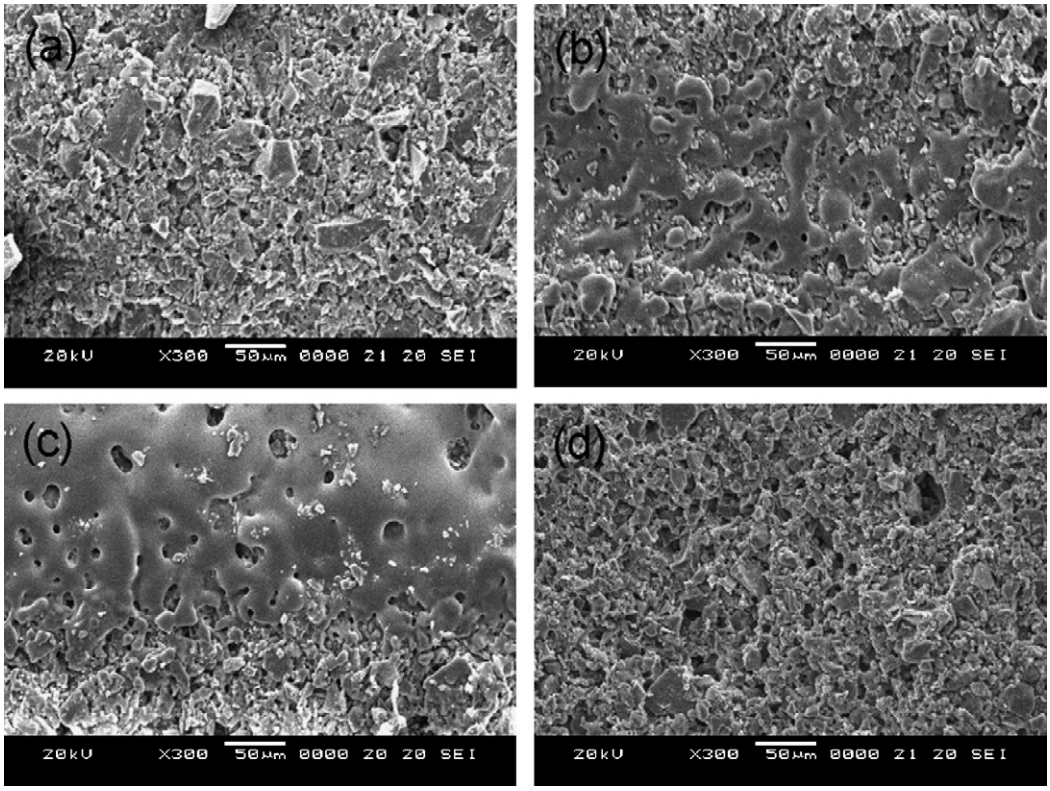

Fig. 5. (a–c) Topographies of the scanned surface obtained from different scanning parameter combinations, and (d) the cross-section of the specimen of (b).

smallest line depth and the weakest binding strength among the three specimens in Fig. 5.

In Fig. 5(b), some of the silica powder in the middle of the surface was melted and bridged. The micrograph in Fig. 5(d), which is similar to the micrograph in Fig. 5(a), reveals the cross-section of the specimen of Fig. 5(b); the silica powder did not melt and there were a lot of pores. Apparently, the surface of the specimen shows that some of the silica powder was melted but the material underneath the surface retained a state of sintering. In Fig. 5(b), obviously, the temperature at the center of the scan line was higher than the melting point of the silica powder. However, the remaining area did not contain the melted silica powder, so its temperature should be close to but lower than the melting point of silica powder. In the present article, Fig. 5(b) is defined as the result of scanning at the critical point. Scanning at this point, as illustrated in Section 2.2, the highest working temperature at the center of the scan line will be close to the melting point of the silica powder.

The micrograph in Fig. 5(c) reveals that more silica powder on the specimen surface was melted when the scan speed was decreased further. The working temperature on most part of the layer surface was over the melting point of the silica powder and the melted powder obstructed most pores between the layers.

The sintering part has more advantages than the fusion part. Although the latter provides a higher binding strength and a greater line depth than the former, it also leads to micro-cracks which reduce the strength. Moreover, the inter-connections between the pores may be obstructed by fused material during the scanning period. Therefore, the part may not be well consolidated by infiltration because the infiltrator will not flow into the closed pores in the partial fusion part. On the contrary, the liquid phase sintering does not lead to micro-cracks, and the inter-connections between the pores will not be obstructed. Therefore, the sintered parts with inter-connective structure can benefit a successful infiltration. Furthermore, the roughness of sintering surface is much better than that of fusion surface. Consequently, the main objective of this paper is to study the laser scanning parameter for the fabrication of ceramic parts by liquid phase sintering.

3.2. Relationship between the laser scanning parameter and the geometry of the scan line

Fig. 6(a) and (b) reveal the trends of the line width and the line depth, respectively when the laser power and the scan speed are varied. Points marked with '□' and '◯' on the constant-scan-speed curves in Fig. 6(a) and (b) are the critical points. The surface temperatures at these points are close to the melting point of silica powder. Increasing the power will lead to the melting of more silica powder and will obtain a scan line containing part of fusion. The line depth is greater than depth achieved at the critical point, so the part is a partial fusion part. Decreasing the power will induce a layer surface temperature lower than the melting point of the silica powder and will obtain a line depth smaller than that achieved at the critical point, so the part fabricated at the critical point will have a maximum sintering depth on the corresponding constant-scan-speed curve. In accordance with the principle of sintering, a higher sintering temperature can

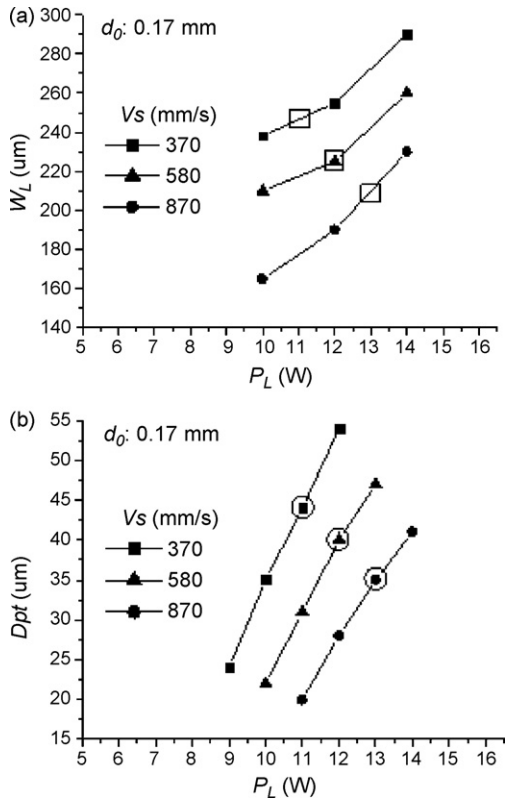

Fig. 6. (a) Influence of the laser power and the scan speed on the line width. (b) Influence of the laser power and the scan speed on the line depth.

induce a higher sintering strength; therefore, owing to the highest sintering temperature, fabricating the part at the critical point should provide the highest sintering strength.

3.3. Relationship between the critical line depth and the scanning parameter

According to the definition of liquid phase sintering mentioned above and the SEM observation, the eight scanning parameter combinations listed in Table 1 have been taken as the working parameter combinations of the critical points. The line width and the line depth are also shown in Table 1. In this paper, the line width and the line depth obtained at the critical point are defined as the critical line width and the critical line depth. Table 1 reveals a significant increase in the critical line depth upon decreasing the scan speed, but the critical line width does not show any significant change. However, both of them increase obviously upon increasing the beam diameter.

Table 1
The critical line depths corresponding to the different scanning parameter combinations.

d_0 (mm)	P_L (W)	V_s (mm/s)	D_{pt} (μm)	W_L (mm)
0.19	12	370	53	0.29
	15	580	47	0.29
	18	870	41	0.31
0.17	11	370	44	0.25
	12	580	40	0.23
	13	870	35	0.21
0.12	7	580	26	0.13
	9	870	21	0.12

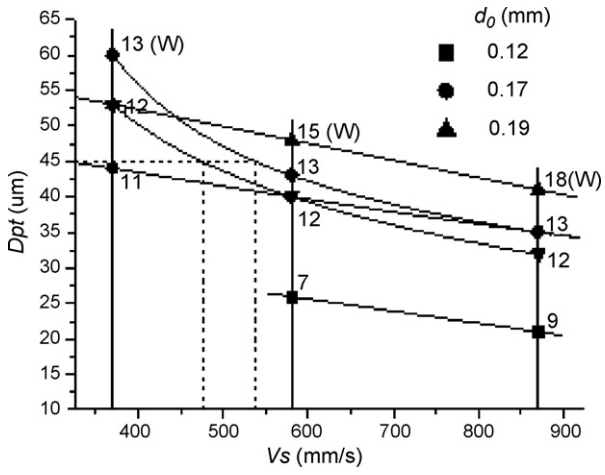

Fig. 7. Relationship between the critical line depth and the scanning parameter.

Fig. 7 shows two constant-laser-power curves and three constant-beam-diameter curves that are built on the additional interpolation and extrapolation of the data listed in Table 1. The constant-beam-diameter curve reveals a linear relation between the critical line depth and the scan speed.

These constant-beam-diameter curves and constant-laser-power curves can be applied to predict the corresponding critical scanning parameter combinations for a specific critical line depth. For instance, corresponding to the critical line depth of 45 μm, many scanning parameter combinations can be obtained from Fig. 7. A horizontal line is plotted from the point of the critical line depth of 45 μm; it intersects the constant-laser-power curves of 12 W and 13 W, respectively. Two vertical lines are plotted from the two intersecting points individually, and they intersect the axis of the scan speed at 475 mm/s and 545 mm/s. By interpolation, the intersecting points occur at the beam diameters of 0.175 mm (D_{df} = 4.15 mm) and 0.18 mm (D_{df} = 4.35 mm), respectively. Consequently, the critical line depth of 45 μm can be generated by scanning at one of these two scanning parameter combinations (P_L = 12 W, V_s = 475 mm/s, d_0 = 0.175 mm or P_L = 13 W, V_s = 545 mm/s, d_0 = 0.18 mm).

4. Conclusion

The present study has established a method to fabricate specially designed specimens for measuring the line depth and the line width of the ultra-thin sintering layer. The feasible minimum line depth is around 20 μm, which can be used to fabricate a part with the layer thickness of 10 μm. By reducing the layer thickness, the stair stepping effect of the part will be improved.

Laser scanning parameters have been optimized for obtaining a part with higher strength. Fabricating a part with the scanning parameter combination of the critical point can achieve the largest sintering depth without melting silica to possess a stronger sintering. The constant-laser-power curves and the constant-beam-diameter curves can be integrated in a diagram to

describe the relationship between the critical scanning parameter combination and the critical line depth. Besides the laser power and the scan speed, this diagram illustrates that a wider variation range of the critical line depth can be obtained by adjusting the beam diameter. By applying this diagram to fabricate sintering parts, a better surface roughness with higher sintering strength may be achieved. It is helpful in improving the quality of parts made by the process of Ceramic Laser Sintering. The mechanical properties of the sintering part will be examined in the future. Inter-connective porous structure formed during the sintering period may benefit the infiltration of the low melting point glass to enhance the strength of the part. The post-treatment of infiltration is one of the most important works of the future.

Acknowledgements

The authors would like to acknowledge the financial support from National Science Council of ROC under project NSC94-2622-E-027-044-CC3. We also thank Mr. Huang-Yin Chen in National Taipei University of Technology for his assistance in specimen fabrication.

References

1. Brady, G. A., Chu, T. M. and Halloran, J. W., Curing behavior of ceramic resin for stereolithography. In *Proceeding of the 7th Solid Freeform Fabrication Symposium*, 1996, pp. 404–410.
2. Brady, G. A. and Halloran, J. W., Stereolithography of ceramic suspensions. *Rapid Prototyping J.*, 1997, **3**, 61–65.
3. Griffith, M. L. and Halloran, J. W., Freeform fabrication of ceramics via stereolithography. *J. Am. Ceram. Soc.*, 1996, **79**, 2601–2608.
4. Doreau, F., Chaput, C. and Chartier, T., Stereolithography for manufacturing ceramic parts. *Adv. Eng. Mater.*, 2000, **2**, 493–496.
5. Agarwala, M. K., van Weeren, R., Bandyopadhyay, A., Whalen, P. J., Safari, A. and Danforth, S. C., Fused deposition of ceramics and metals: an overview. In *Proceeding of the 7th Solid Freeform Fabrication Symposium*, ed. D. L. Bourell, 1996, pp. 385–392.
6. Bellini, A., Shor, L. and Guceri, S. I., New developments in fused deposition modeling of ceramics. *Rapid Prototyping J.*, 2005, **11**, 214–220.
7. Klosterman, D., Chartoff, R., Osborne, N. and Graves, G., Automated fabrication of monolithic and ceramic matrix composites via laminated object manufacturing (LOM). In *Proceeding of the 8th Solid Freeform Fabrication Symposium*, ed. D. L. Bourell, 1997, pp. 537–549.
8. Klosterman, D., Laminated Object Manufacturing (LOM) of advanced ceramic and composites. In *Proceeding of the 7th International Conference on RP*, 1997, pp. 43–50.
9. Klosterman, D., Chartoff, R., Graves, G., Osborne, N., Lightman, A., Hanand, G. and Bezeredi, A., Direct fabrication of ceramics and composites through laminated object manufacturing (LOM). *Materials and Process Affordability: Keys to the Future*, 1998, **43**, 693–705.
10. Subramanian, P. K., Vail, N., Barlow, J. W. and Marcus, H. L., Selective laser sintering of alumna with polymer binders. *Rapid Prototyping J.*, 1995, **1**, 24–35.
11. Klocke, F. and Wirtz, H., Selective laser sintering of zirconium silicate. In *Proceeding of the 9th Solid Freeform Fabrication Symposium*, ed. D. L. Bourell, 1998, pp. 605–612.
12. Wirtz, H., Selektives Lasersintern von Keramikformschalen für Giessanwendungen, Ph.D. thesis, RWTH Aachen, Germany, 2000.
13. Sachs, E. M., Haggerty, J.,S., Cima, M. J. and Williams, P. A., Three dimensional printing techniques. United States Patent 5,204,055 (1993); 5,340,656 (1994).
14. Sachs, E.,M., Curodeau, A., Fan, T., Bredt, J. F., Cima, M. J. and Brancazio, D., Three dimensional printing system. United States Patent 5,807,437 (1998).
15. Grau, J., Moon, J., Uhland, S., Cima, M. and Sachs, E., High green density ceramic components fabricated by the slurry-based 3DP process. In *Proceeding of the 8th Solid Freeform Fabrication Symposium*, ed. D. L. Bourell, 1997, pp. 371–378.
16. Tang, H. H., Method for rapid forming of a ceramic work piece. United States Patent No. 6,217,816 (2001).
17. Tang, H. H., Direct laser fusing to form ceramic parts. *Rapid Prototyping J.*, 2002, **8**, 284–289.
18. Tang, H. H. and Yen, H. C., Ceramic parts fabricated by ceramic laser fusion. *Mater. Trans. J. Jpn. Ins. Met.*, 2004, **45**, 2744–2751.
19. Tang, H. H., Building ultra-thin layers by ceramic laser sintering. *Mater. Trans. J. Jpn. Ins. Met.*, 2006, **47**, 889–897.
20. Yen, H. C., Tang, H. H. and Chen, T. C., Fabricating workpiece with 1700 dpi vertical resolution by ceramic laser sintering. In *Proceedings of the 3rd International WLT International Conference on Laser in Manufacturing*, 2005, pp. 245–249.
21. Yen, H. C. and Tang, H. H., Developing a paving system for fabricating ultra-thin layers in ceramic laser rapid prototyping. *Int. J. Adv. Manuf. Technol.*, 2008, **36**, 280–287.